FRANCIS TURBINE SURGE : DISCUSSION AND DATA BASE

Thierry Jacob and Jean-Eustache Prénat
IMHEF-EPFL, av de Cour 33, 1007 Lausanne, Switzerland

0. Background

A system is considered as stable in sustained operating conditions if the response to unavoidable disturbances does not endanger its safety. Normal disturbances of hydraulic turbines are pressure fluctuations [3, 5, 10], influenced by machine design, operating conditions and by the dynamic response of the water conduits and rotating components. They may be associated with mechanical fluctuations of shaft torque, rotational speed, hydraulic load on guide vanes etc. as well as with vibrations.
Low frequency pressure fluctuations are a special threat to stability of operation because they may propagate to the whole piping system and cause hydraulic resonance. They may also excite sub-synchronous free oscillations of the prototype rotating machinery. They occur typically between 0.2 and 3 times the runner rotational frequency.
In Francis turbines, a strong runner outlet swirl develops in off-design conditions and induces flow instabilities in the draft tube. This draft tube surge is the most commonly identified phenomenon among low frequency pressure fluctuations. In addition, draft tube cavitation may change the natural frequencies of the hydraulic system.
In the following pages, we will discuss various aspects of draft tube surges. Our purpose is to establish guidelines for the interpretation of pressure fluctuations. The discussions are based on test results from over twenty turbine models and three prototypes from different manufacturers, with specific speeds n_{QE} ranging from 0.074 to 0.320.

1. Classification of draft tube pressure surges

1.1. OPERATING RANGE

Turbine operation parameters are the energy and discharge coefficients E_{nD} and Q_{nD}. The reference coefficients are at best efficiency. The reference elevation for Thoma number σ is the runner outlet at the band.

$$E_{nD} = \frac{E}{n^2 D^2} \quad ; \quad Q_{nD} = \frac{Q}{nD^3} \quad ; \quad n_{QE} = \frac{Q_{nD}^{1/2}}{E_{nD}^{3/4}} \quad ; \quad \sigma = \frac{NPSE}{E} \qquad (1)$$

Figure 1 is the schematic operating range of a Francis turbine. Constant guide vane angle lines and efficiency contours are set in the hydraulic energy-discharge diagram for a constant rotational speed. The turbine is defined by its best efficiency specific hydraulic energy (a) and discharge (b), and a rated specific hydraulic energy of the project (c), which may be different from best efficiency.
The range of operation is limited by the minimum guide vane angle for sustained operation (d), the maximum guide vane angle (e), the maximum (f) and minimum (g) specific hydraulic energies of the project and by the maximum generator power (h).
Pressure fluctuations in the draft tube are observed at the rated energy coefficient (c), from minimum to maximum guide vane angle. A waterfall diagram displays the Fourier

E. Cabrera et al. (eds.), Hydraulic Machinery and Cavitation, 855–864.

transform amplitude of pressure fluctuations as a function of frequency and discharge coefficient. Pressure fluctuations are made non-dimensional by the specific hydraulic energy. Fluctuation frequencies are made non-dimensional by the rotational frequency. The following domains are defined within the operating range, see also [3] :

1 very low discharge operation;
2 part load operation;
3 high partial load operation;
4 operation around best efficiency;
5 full-load operation.

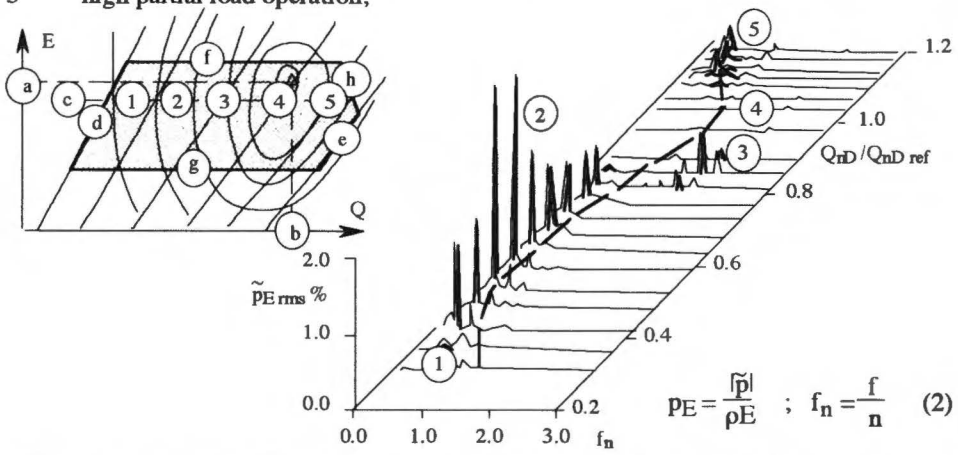

Figure 1. Francis turbine hill-chart and waterfall diagram of pressure fluctuations in the draft tube cone

1.2. DRAFT TUBE PRESSURE SURGES

1.2.1. *Part load precession*

Label (2) in the waterfall diagram of figure 1 marks the pressure fluctuations associated with the part load precession. The precession is the motion of a center of rotation around a fixed axis. At part load, the diverging geometry of the draft tube and the draft tube elbow induce a forced precession of the swirling flow at the runner outlet. When Thoma number is small enough, a vapor cavity forms along the vortex center. The helical shape and circular motion of this cavity are evidences of the precession.

The precession generates a rotating field of velocity and pressure fluctuations in the draft tube cone. Defaults in axial symmetry, mostly due to the draft tube elbow, cause a hydraulic excitation at the precession frequency.

Similitude considerations show that the precession frequency can be made non-dimensional by the rotational frequency, and that the excitation magnitude can be made non-dimensional by the turbine specific hydraulic energy. Although the frequency could theoretically vary in a great range, most Francis turbines feature a part load precession frequency of about :

$$\frac{f_p}{n} \approx 0.26 \pm 20\ \% \qquad (3)$$

An unusual turbine design can lead to a different precession frequency. Relative frequencies as high as $f_p/n = 0.4$ were found on upgraded turbines.

Pressure fluctuations associated with the part load precession are influenced by turbine design and by the dynamic response of the test circuit or prototype water conduits. If distortions due to dynamic responses of the test circuit and rotating components are small, the order of magnitude of pressure fluctuations at position (1), figure 2, is about :

$$\tilde{p}_{E\,rms} \approx \frac{n_{QE}}{5} \pm 50\ \% \qquad (4)$$

Harmonic frequencies of the precession often appear in the spectral data. They usually cause little or no excitation. Multiple vortex precession [12] sometimes occurs at very low discharge, see label (1) in figure 1. Associated amplitudes are generally small.

1.2.2. *Free oscillations of draft tube flow*

A large vapor cavity [6] forms at the runner outlet, due to the residual swirl and the low pressure level. The water plug in the draft tube oscillates against this elastic volume. System constants are the inertia I of the water plug and the cavitation compliance C.

$$f_0 = \frac{1}{2\pi\sqrt{IC}} \quad ; \quad I = \int \frac{dL}{A} \quad ; \quad C = -\frac{\partial V_{vap}}{\partial NPSE} \tag{5}$$

The dotted line in the waterfall diagram of figure 1 marks the frequency of free oscillations. It is smallest at part load and at full load, when the volume of draft tube cavitation is maximum. In this case, the frequency of free oscillations gets very close to the part load precession frequency and draft tube resonance is responsible for the high pressure fluctuation amplitudes.

For a usual draft tube design and a reference Thoma number such as $\sigma \cdot E_{nD} = 1$ for operation at the best efficiency E_{nD}, we can expect the minimum value of the draft tube free oscillations frequency at part load to be close to the precession frequency.

$$\sigma = \frac{1}{E_{nD}} \rightarrow f_{0\,min} \approx f_p \pm 50\ \% \tag{6}$$

For a first approximation, the influences of Thoma number and energy coefficient are :

$$\frac{\partial(f_0/n)}{\partial\sigma} \approx 20 - 35\sqrt{n_{QE}} \pm 50\% \quad ; \quad \frac{\partial(f_0/n)}{\partial(E_{nD}/E_{nDref})} \approx 0.75 \pm 50\% \tag{7}$$

The frequency of free oscillations at full load varies in a wide range according to the turbine design. Its partial derivative to Thoma number is approximately the same as at part load. We could not find a coherent statistic on the magnitude and sign of the partial derivative to energy coefficient.

The water compressibility contributes to the compliance, but is not scalable from model to prototype. This introduces errors in the prediction of free oscillations frequency around best efficiency when the vapor volume is small, or in cases where the draft tube is specially long. In normal cases of part load and full load operation with short draft tubes, the frequency of free oscillations in model tests was not changed significantly by the injection of cavitation nuclei, or even by testing in open circuit mode.

1.2.3. *High partial load instability*

Label (3) in the waterfall diagram of figure 1 marks the pressure fluctuations associated with the high partial load instability, which sometimes occurs between 70 and 90 % of best efficiency discharge. Its physical mechanism is not precisely known. It seems to be connected with pressure waves traveling along the surface of the draft tube vortex cavity, and excited by the passage of the precessing vortex in the draft tube elbow. High partial load instabilities induce large pressure fluctuations in the spiral case and draft tube elbow. They can be responsible for strong vibrations. They are eliminated by air admission flows smaller than 0.1 % of best efficiency discharge.

1.2.4. *Self-amplified pulsations*

Label (5) in the waterfall diagram of figure 1 marks the pressure fluctuations associated with the full load pulsations. When the partial derivatives of cavitation compliance versus discharge and energy have the same sign, the damping of draft tube free oscillations may become negative. This can occur at very low discharges or at full load. Like draft tube free oscillations, the frequency of full load pulsations can be made non-dimensional by the rotational frequency. The amplitude has no real meaning, as this fluctuation is likely to grow catastrophically, depending on the penstock response.

2. Observation of pressure fluctuations

2.1. POSITION OF PRESSURE TRANSDUCERS

The analysis is based on signals from pressure transducers located in the draft tube cone and elbow, where most disturbances are generated. The reference pressure signal is on the inner side of the elbow (1), where amplitudes are often greatest. To allow a separation between rotating and synchronous surges, more transducers are placed at the same elevation, around the draft tube cone (2, 3). The angular position is not important, but immediate interpretation is easier if one is placed on the outer side of the elbow (2).
Spiral case inlet pressure fluctuations (4) are distorted by standing wave effects, characteristic of the test circuit. To evaluate and correct these distortions, additional pressure signals (5, 6) are collected on the feed pipe.
The measurement of torque fluctuations gives a general idea of power fluctuations to be expected on the prototype, even if this observation is not directly transposable.

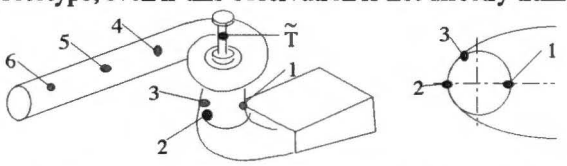

Figure 2. Transducer positions for measurements of stability of operation

2.2. DISCUSSION OF DRAFT TUBE CONE PRESSURE FLUCTUATIONS

2.2.1. *Synchronous and rotating surges*

If we compare the pressure signals from transducers 1, 2 and 3 around a transverse section of the draft tube cone, the magnitudes are the same and the fluctuations are in phase for the draft tube free oscillations, the base frequency of the high partial load instability and for the full load pulsation.
The part load precession and the secondary peak of the high partial load instability have different amplitudes and phase angles within a transverse section of the draft tube cone. These rotating surges can be simplified with an appropriate analysis.

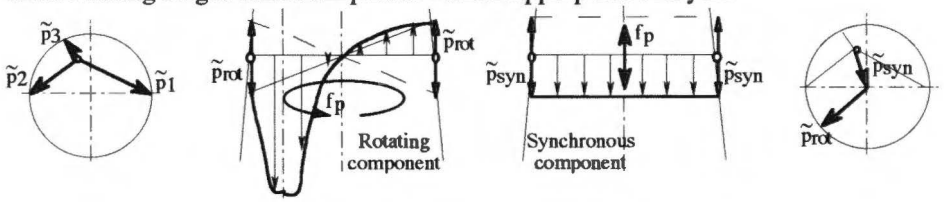

Figure 3. Rotating surge analysis [1]

The observation of pressure fluctuations associated with rotating surges can be quite different, depending on the transducer position. In the example of figure 3, a diagnosis based on the signal from transducer 3 alone would be misleading. Rotating surge analysis can be done on two or more pressure signals from the same circular transverse section of the draft tube cone. The pressure fluctuation is split into two components uniform along the draft tube circumference : $\tilde{p}_{rot}$ is purely rotating and $\tilde{p}_{syn}$ is purely synchronous. With this method, we can compute the pressure fluctuation amplitude at any position around the draft tube cone as the vectorial sum of $\tilde{p}_{syn}$ and $\tilde{p}_{rot}$.
Marginal peaks such as harmonics of the precession cannot be processed this way, but they are less important in the evaluation of stability of operation.

2.2.2. *Discussion of the rotating component of the part load precession*

For a given runner and draft tube cone, $\tilde{p}_{rot}$ is not influenced by Thoma number, by the design of the draft tube elbow or by the length of the feed pipe.

Figure 4 shows the evolution of $\tilde{p}_{rot}$ versus discharge coefficient for different specific speeds. The magnitude of $\tilde{p}_{rot}$ increases with n_{QE}.

The rotating surge analysis is done 0.5 and 1.5 runner diameters below the guide vane center-line. In the top of the draft tube cone, the magnitude of $\tilde{p}_{rot}$ is maximum around 50 % of best efficiency discharge, then drops steadily to zero in the vortex-free region.

In the bottom of the draft tube cone, $\tilde{p}_{rot}$ first rises, then drops around 60 % of best efficiency flow, then goes to a maximum and dies down in the vortex-free region. It does not seem easy to interpolate $\tilde{p}_{rot}$ along the height of the cone, or to tell which elevation is most representative of the precession.

Model measurements of pressure fluctuations must be done at the position where the prototype draft tube is accessible. If an arbitrary elevation must be chosen, it can be one runner diameter below the guide vane center-line, where the model is always accessible.

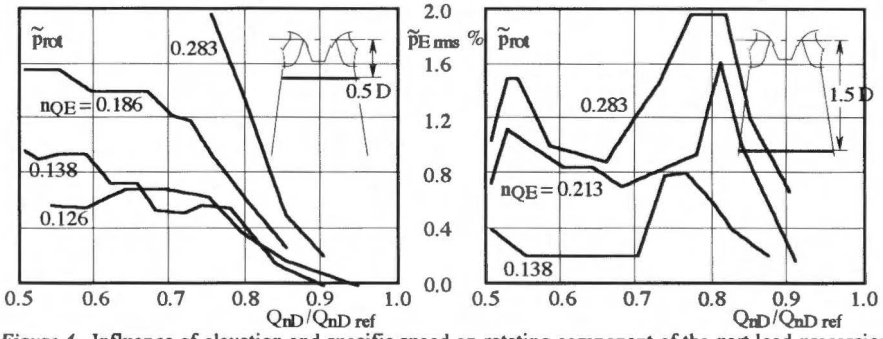

Figure 4. Influence of elevation and specific speed on rotating component of the part load precession

2.2.3. *Discussion of the synchronous component of the part load precession*

$\tilde{p}_{syn}$ was for some time considered as representative of the excitation. Conceptually, it is very close to the passage of the vortex in the draft tube elbow. However, $\tilde{p}_{syn}$, as the pressure fluctuation averaged over the transverse section of the cone, is the sum of the excitation and of the system response, which may vary according to the boundary conditions. Figure 5 shows the pressure fluctuations at the spiral case inlet and $\tilde{p}_{syn}$ for an $n_{QE} = 0.138$ turbine. The correlation between the two amplitudes is excellent.

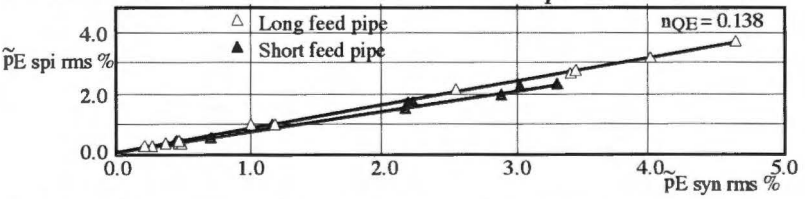

Figure 5. Pressure fluctuation at spiral case inlet and synchronous component of the part load precession

The magnitude of $\tilde{p}_{syn}$ is constant from the top to the bottom of the draft tube cone, over the whole vertical extent of the vapor-filled cavity.

The test was done once with a 6.7 m feed pipe and once with only 3.1 m (19.7 and 9.1 D). The spiral case pressure fluctuation was reduced by 39 % and $\tilde{p}_{syn}$ by 29 % for the 54 % reduction in pipe length. It seems difficult to correct such distortions due to the dynamic response of the test circuit, if $\tilde{p}_{syn}$ is to be used to estimate the excitation.

The gain of $\tilde{p}_{spi}$ to $\tilde{p}_{syn}$ was also found to vary with Thoma number, test head and draft tube depth. No satisfying correlation could be established with the specific speed.

3. Magnitude of hydraulic excitations

3.1. DISTORTIONS DUE TO STANDING WAVES

Local impedances [13] determine the amplitude of pressure fluctuations that develop in a piping system in response to a hydraulic excitation. Pressure signals measured on the feed pipe of a Francis turbine will depend on the position of measurement along the pipe. The amplitude at the spiral case inlet will be influenced by the feed pipe length and wall stiffness. These distortions due to standing waves in the piping system must be corrected for an estimation of the excitation magnitude. The observations of pressure fluctuation amplitudes alone is not sufficient.

The active acoustic power is the energy flow associated with a hydraulic oscillation. It combines pressure and kinetic energies. As it is not influenced by standing waves in the piping, it represents the excitation magnitude more adequately than spiral case inlet pressure fluctuation amplitudes.

The active acoustic power is equal to the real part of the pressure fluctuation times the conjugate of the discharge fluctuation. Its value does not depend on the position along a uniform length of friction-less pipe. It can be positive or negative, indicating the direction of the energy flow. This allows an identification of disturbances generated by the circuit such as feed pump noise, pipe movements etc.

The active acoustic power can also be expressed as the scalar product of pressure and discharge fluctuation vectors, considering their phase shift φ :

$$\text{Real}(\tilde{p}\bullet\tilde{q}^*) = |\tilde{p}|\bullet|\tilde{q}|\bullet\cos\varphi \qquad (8)$$

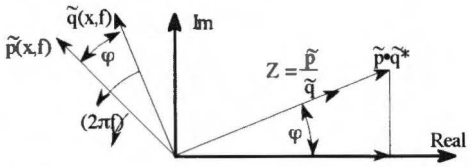

Figure 6. Construction of the impedance and active acoustic power in the complex plane

3.2. SOURCE PRESSURE MODELING OF EXCITATIONS

Replacing the discharge fluctuation $\tilde{q}$ by $\tilde{p}/Z$, we see that the result of acoustic power processing is a correction of the influence of local impedance on the local pressure fluctuation amplitude. Normalizing the equation by the reference impedance Z_0, we obtain a source pressure $\tilde{p}_{src}$ [9].

The source pressure, propagating in reflection-free conditions, would carry the same active power as the actual hydraulic fluctuation :

$$\text{Real}(\tilde{p}\bullet\tilde{q}^*) = \text{Real}\left(\frac{\tilde{p}\bullet\tilde{p}^*}{Z^*}\right) = |\tilde{p}|^2 \bullet \frac{|\text{Real}(Z)|}{|Z|^2} \qquad (9)$$

$$\tilde{p}_{src} = \sqrt{Z_0\bullet\text{Real}(\tilde{p}\bullet\tilde{q}^*)} \quad ; \quad \tilde{p}_{src} = |\tilde{p}| \bullet \frac{\sqrt{Z_0\bullet|\text{Real}(Z)|}}{|Z|} \qquad (10)$$

The source pressure associated with the part load precession is influenced by the turbine design and operating parameters, but the compensation of reflections due to the circuit reduces the scatter. Between 0.5 and 0.8 Q_{nDref} for operation at E_{nDref} and $\sigma\bullet E_{nD} = 1$, expectable excitation magnitudes are :

$$\tilde{p}_{E\ src\ rms} \approx 0.01 \pm 30\ \% \quad \text{at} \quad f_p \approx 0.26\ n \pm 20\% \qquad (11)$$

The amplitude of draft tube pressure fluctuations is correlated with n_{QE}, see figure 4, but this influence is not found in the source pressure estimated at the spiral case inlet.

3.3. DISCUSSION

The use of active oscillatory power to isolate the magnitude of disturbances from the environment response is so widespread in other fields of engineering that it is hardly questionable as a concept. The source pressure formulation is equivalent to the source vectors used in association with a transfer matrix to represent the disturbances generated by a circuit element, when the pressure and discharge components of the vector are related by the reference acoustic impedance Z_0.
The problem with the application of acoustic power methods to turbines is that most disturbances are generated in the draft tube cone and elbow, but the suitable position for the evaluation of the source pressure is the spiral case inlet. There are possibilities of oscillatory power leakage between the emission and the measurement position. The outlet through the draft tube is not a problem : its impedance is imaginary if the draft tube opens in a tank with a sufficiently large free surface, and it is very hard to force acoustic power in this direction. Leakage to the turbine attachments could occur on models with excessive deformations, but this should not be the case.

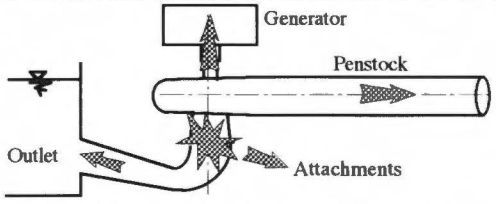

Figure 7. Outflow of oscillatory energy from the turbine

A more likely source of trouble is the exchange of oscillatory power with the rotating machinery, if there are fluctuations of rotational speed. In one case, we could trace discrepancies in source pressure estimations at different test heads to changes in torque fluctuations [9]. A future progress in testing technique will be the use of quick-response tachometers for the measurement of mechanical oscillatory power on the turbine shaft.

4. Prediction of prototype pressure fluctuations

4.1. IMPEDANCE ANALYSIS OF PROTOTYPE INSTALLATION

The eventuality of resonance of the prototype water conduits is investigated in the frequency domain, using linear transmission theories such as impedance methods [13]. The modeling of the plant is usually confined to the piping system, computing impedances from all ends. In the scope of the discussion in (2.3), the electric network and generator should also be included in the impedance analysis [2]. The dynamic model is excited with an arbitrary pulsed discharge at the outlet of one of the runners, and we compute the response in pressure at all units. The absolute amplitude has no meaning at this stage, as the excitation is not realistic.
An important parameter of the simulation is the cavitation compliance C [3, 6], estimated from model tests as in equation (5) and transposed to prototype dimensions and operating conditions. Figure 8 shows the response of a prototype to an arbitrary 1 % pulsed discharge excitation and computed for two values of the cavitation compliance. With C_1, the first resonance frequency is close to the part load precession frequency f_p. The installation of fins on the draft tube wall changed the compliance to C_2. The danger of part load resonance was suppressed. This solution was put to practice on a field case of instability and gave full satisfaction [8].

The cavitation compliance can change very much from one turbine design to another, and it seems difficult to estimate its value from global parameters. The compliance factor at part load and at full load is often in the range of :

$$C_{ED} = \frac{C \bullet E}{D^3} \approx 0.1 \ldots 2 \tag{12}$$

In addition to the forced response presented here, impedance methods cover the identification of free oscillation modes, including damping factors. The computed attenuation is generally much smaller than the actual and can be difficult to interpret.

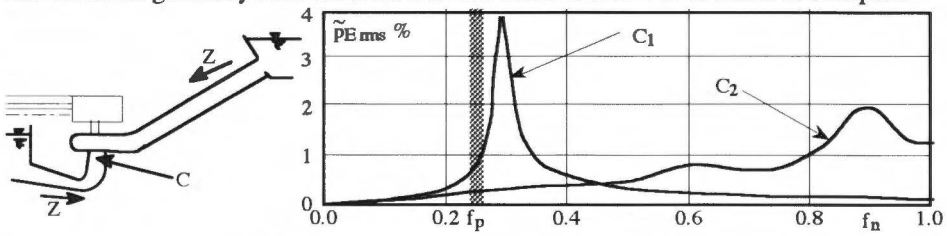

Figure 8. Impedance analysis including cavitation compliance

4.2. TRANSPOSITION OF EXCITATIONS DUE TO THE TURBINE

Excitations due to the turbine are formulated as source pressures, which are transposed to the prototype specific hydraulic energy. Excitation frequencies are scaled to the prototype rotational frequency. The pressure fluctuation $\tilde{p}_{spi}$ at the prototype spiral case inlet must meet two requirements : the local impedance Z_{spi} resulting from the penstock dynamic response and the source pressure $\tilde{p}_{src}$. Reversing equation (10), we obtain :

$$\tilde{p}_{spi\ M \rightarrow P} = \tilde{p}_{src\ M} \bullet \frac{(\rho E)_P}{(\rho E)_M} \bullet \frac{|Z_{spi}|}{\sqrt{Z_0 \bullet |Real(Z_{spi})|}} \tag{13}$$

The result of this transposition is compared with field measurements on figure 9. The agreement is good at part load. This method is not suitable for the prediction of full load pulsation amplitudes, as these are self-amplified fluctuations.

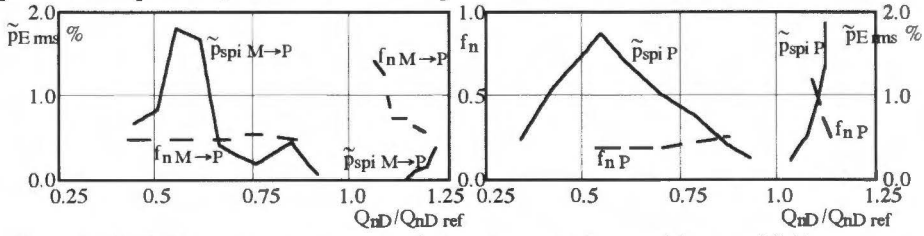

Figure 9. Simulated prototype response to excitations transposed from model tests and field measurement

4.3. DISCUSSION

Hydro power installations are built to minimize energy losses. The real part of a penstock impedance is often very small. From equation 13, we see that errors in the estimation of $Real(Z_{spi})$ can significantly change the predicted pressure fluctuation amplitude. As the modeling of pipe friction is not accurate, this is a limitation of the method.
Possible exchanges of oscillatory power with the rotating machinery were mentioned in the discussion of 3.3 on the estimation of the excitation magnitude. Accordingly, if the oscillatory power on the turbine shaft can be measured, the resulting excitation power is the sum of the feed pipe and shaft active powers. As active powers are scalar quantities,

there are no problems of phase for the addition of the two. A source pressure can then be formulated in the region of the physical excitation, i.e. the draft tube cone and elbow. The penstock and rotating masses impedances combine in a runner outlet impedance from which the local response is computed. At part load, this local pressure fluctuation is the synchronous component of the draft tube surge. The rotating component must still be introduced with due regard to phase for a realistic simulation.

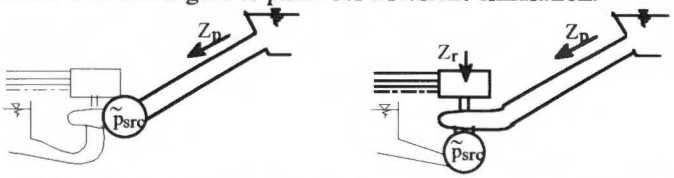

Figure 10. Modeling of responses of the penstock alone or of both penstock and rotating machinery

A prediction of excessive pressure fluctuations makes it possible to optimize stabilizing devices before the prototype is erected.
Structures such as cross-trees, tripods, central cylinders or piles can be installed in the draft tube cone to disorganize swirling flow [7]. These devices reduce the efficiency. In many cases, they were broken after a few hours of operation. Structures in the center of the draft tube cone are effective against the full load pulsation.
Fins on the draft tube wall can reduce the amplitude of pressure fluctuations at part load with small efficiency losses if their position and setting angle are well chosen. In one case, the stabilizing effect of fins was identified as a reduction of the cavitation compliance (figure 8) and the suppression of the synchronous component of the part load precession. The rotating component was not modified [8].
Longer runner cones [11] reduce the reverse flow in the central region of the draft tube cone. In some cases, this reduced the full load pulsation.
Air admission through the runner cone [7] increases the volume of the draft tube cavity. This increases the cavitation compliance and lowers the draft tube free oscillations frequency. Draft tube resonance can be eliminated this way. Air admission can also induce draft tube resonance when the free oscillations frequency without air is higher than excitation frequencies. In some cases, air admission is not effective at full load. It is advisable to have some control over the air inflow valve.
Penstock resonance can be reduced using accumulators or Helmholtz resonators. This can be a good solution for small scale power plants. Active control is considered [4] to govern the spiral case inlet impedance or reduce the excitation power.

5. Conclusions

Most stability problems of Francis turbines can be identified as one of the following :
- Rotating surges related to the part load precession, with possible draft tube resonance;
- High partial load instability, bursts of pressure fluctuations and vibrations;
- Full load pulsation, self-amplified surge.

These phenomena have been described in terms of pressure pulsations. Advanced analysis tools provide the basis of a quick and easy diagnosis of stability of operation. Frequencies and magnitudes can be compared to the typical values listed in this paper.
The excitation magnitude is estimated through the active power of the hydro-acoustic fluctuations in the feed pipe of the model turbine in laboratory test. This method should be improved with the inclusion of oscillatory power exchanges with the generator.
The prediction of prototype pressure fluctuation is done by numerical simulation of the excitation on an impedance model of the plant piping system.

Symbols

A	Cross-sectional area	m^2
C	Cavitation compliance, see equation (5)	m^4s^2
C_{ED}	Cavitation compliance factor, see equation (12)	
D	Runner diameter	m
E	Specific hydraulic energy of turbine	J/kg
E_{nD}	Energy coefficient, see equation (1)	
f	Frequency	Hz
f_n	Frequency made non dimensional by the rotational frequency	
f_p	Precession frequency	Hz
f_0	Draft tube free oscillations frequency	Hz
I	Inertia of water column	m^{-1}
NPSE	Net positive suction energy of turbine reference elevation at runner outlet periphery	J/kg
n	Rotational frequency of turbine	rev/s
n_{QE}	Specific speed, see equation (1)	
$\tilde{p}$	Pressure fluctuation; for the considered frequency, coefficient of the Fourier transform of the pressure signal	N/m^2
$\tilde{p}_E$	Pressure fluctuation amplitude factor, see equation (2) (rms = effective value)	
$\tilde{p}_{rot}$	Rotating component of draft tube rotating surge	N/m^2
$\tilde{p}_{syn}$	Synchronous component of draft tube rotating surge	N/m^2
$\tilde{p}_{spi}$	Pressure fluctuation at spiral case inlet	N/m^2
$\tilde{p}_{src}$	Source pressure associated with active acoustic power, see equation (10)	N/m^2
Q	Discharge	m^3/s
Q_{nD}	Discharge coefficient, see equation (1)	
$\tilde{q}$	Discharge fluctuation	m^3/s
V_{vap}	Vapor volume	m^3
Z	Hydro-acoustic impedance	$N/m^4/s$
Z_{spi}	Spiral case inlet impedance	$N/m^4/s$
Z_0	Reference acoustic impedance (propagation constant of pipe)	$N/m^4/s$
ρ	Mass per unit volume	kg/m^3
σ	Thoma number, reference elevation at runner outlet periphery	
$\ldots_{ref}$	Reference value (for E_{nD} and Q_{nD} : best efficiency operation)	
$\ldots^*$	Complex conjugate	
$\ldots_M$	Model quantity	
$\ldots_P$	Prototype quantity	
$\ldots_{M\rightarrow P}$	Transposed from model to prototype	
...	Accessory symbols are defined as they appear in the text.	

References

[1] ANGELICO G., MUCIACCIA F., ROSSI G. : Part load behaviour of a turbine : a study on a complete model of hydraulic power plant. IAHR Symposium Montréal (1986)

[2] CATTANEI A., CAPOZZA A. : Analysis of a numerical model for the oscillatory properties of a Francis turbine group. IAHR WG. Ljubljana (1995)

[3] DÖRFLER P. : Francis turbine surge prediction and prevention. Waterpower '85, Las Vegas (1985)

[4] FANELLI M. : Research on off-design behaviour of Francis turbines : an overview of present state, difficulties, open problems, needs and strategies. IAHR W.G. Milan (1991)

[5] FISHER R.K., ULITH P. : Comparison of draft tube surging of homologous scale models and prototype Francis turbines. Voith Research and Construction vol 28e (1982)

[6] FRANC J.P. et al. : La Cavitation, mécanismes physiques et aspects industriels. Presses Universitaires de Grenoble (1995)

[7] GREIN H. : Vibration phenomena in Francis turbines : their causes and prevention. IAHR Symposium Tokyo (1980)

[8] JACOB T., PRENAT J.E., BUFFET G., WINKLER S. : Improving the stability of operation of a 90 MW Francis turbine. Hydropower, Barcelona (1995)

[9] JACOB T., PRENAT J.E., WINKLER S. : Acoustic power analysis for the stability of operation of Francis turbines. IAHR WG, Ljubljana (1995)

[10] KERKAN V., BAJD M., DJELIC V., LIPEJ A., JOST D. : Model and prototype draft tube pressure pulsations. IAHR W.G. Ljubljana (1995)

[11] THICKE R.H. : Methods of controlling turbine draft tube vibrations and stability. Canadian electrical association, hydraulic power section (1980)

[12] WAHL T. : Draft tube surging times two : the twin vortex phenomenon. Hydro Review, feb (1994)

[13] ZIELKE W. : Unsteady one-dimensional flows in complex networks and pressurized vessels: Vibrations and resonance in hydraulic systems. Von Karman Institute for Fluid Dynamics (1980)